Available online at www.sciencedirect.com

ScienceDirect

Mendeleev Commun., 2024, **34**, 232–234

Mendeleev Communications

A new photocatalyst based on layer-ordered anatase nanoparticles doped with manganese

Irina N. Zhukova,[a] Artem Yu. Tatarenko,[a] Artemii N. Beltiukov,[b] Alexey A. Sadovnikov[c,d] and Olga V. Boytsova*[a,e]

[a] *Department of Materials Science, M. V. Lomonosov Moscow State University, 119991 Moscow, Russian Federation. E-mail: boytsova@gmail.com*

[b] *Udmurt Federal Research Center, Ural Branch of the Russian Academy of Sciences, 426067 Izhevsk, Russian Federation*

[c] *N. S. Kurnakov Institute of General and Inorganic Chemistry, Russian Academy of Sciences, 119991 Moscow, Russian Federation*

[d] *A. V. Topchiev Institute of Petrochemical Synthesis, Russian Academy of Sciences, 119991 Moscow, Russian Federation*

[e] *Department of Chemistry, M. V. Lomonosov Moscow State University, 119991 Moscow, Russian Federation*

DOI: 10.1016/j.mencom.2024.02.024

A novel photocatalyst based on Mn-doped carbon-containing TiO_2 layered metastructure has been successfully prepared. For the first time, the exact distance between layers in highly oriented anatase arrays produced with the assistance of PEG 400 was determined. The synthesis of a series of single-phase $Ti_{1-x}Mn_xO_2$ samples with a layer-ordered anatase structure and a doping degree from 0.0 to 2.0% was first carried out by annealing crystalline NH_4TiOF_3 together with a Mn-containing precursor in an air atmosphere at 450 °C for 2 h.

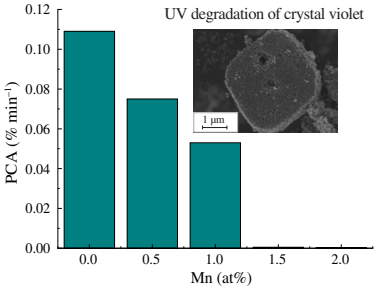

Keywords: anatase, mesocrystal, layered structures, photocatalyst, Mn-doped.

The photocatalytic activity (PCA) of titanium dioxide depends on the crystal structure, surface area, crystallite size, concentration of surface hydroxyl groups, *etc.* Due to its photocatalytic properties, titanium dioxide has many diverse applications, for example: water and air purification, destruction of organic contaminants, neutralization of microorganisms and pathogenic bacteria, photocatalytic lithography, coating of metals to prevent corrosion, H_2 synthesis, fabrication of electrodes for solar cells, production of self-cleaning, hydrophilic and antibacterial functional coatings.[1,2] Therefore, TiO_2 is currently being intensively studied, including with the aim of increasing its efficiency. This can be done in various ways, such as changing the particle size, modifying (decorating) the surface, manufacturing composite materials with spatial separation of charges, alloying with metals and non-metals.[3–5] Previously,[6] TiO_2:Mn nanoparticles were synthesized by the sol–gel method followed by annealing at 500 °C. It was found that when the dopant content is 1 and 2 at%, titanium dioxide is present in the form of a mixture of anatase and rutile phases. When measuring PCA, the powders demonstrated degradation of 100% of Congo red and 80% of methylene blue after 1 h of exposure to sunlight. Such characteristics indicate the great potential of TiO_2 for industrial wastewater treatment. TiO_2–MnO_2 powders can be synthesized using the hydrothermal method. For example,[7] it has been shown that doping with manganese leads to an increase in light absorption in the visible region, and the degree of light absorption increases with increasing Mn concentration. However, higher absorption does not always lead to improved PCA. This is because the number of photogenerated electrons increases with increasing light absorption, but when their concentration is high, they can quickly recombine with holes, which ultimately leads to a significant decrease in the number of free electrons. The highest PCA is achieved at 4 wt% Mn. This sample at a concentration of 0.1 g dm^{-3} promoted the mineralization of 90% of phenol with an initial concentration of 10 mg dm^{-3} in 7 h when irradiated with UV-visible light ($300 < \lambda < 600$ nm). To reduce costs, the material must be modified so that there is enough light in the visible spectrum for it to work. To achieve this result, TiO_2 can be doped with metals and non-metals to reduce its band gap. Manganese may be a good candidate because MnO_2 has photocatalytic properties[8] and the addition of Mn cation to the structure can provide absorption in the visible range.[9] However, there is still no data on the production of manganese-doped TiO_2 in the form of mesocrystals. In this work, photoactive Mn-doped titanium dioxide mesocrystals in the anatase form were demonstrated for the first time.

Using the described method,[†,10,11] a series of layered microstructures $Ti_{1-x}Mn_xO_2$ was obtained, in which Mn replaces

[†] All chemical compounds used in the synthesis were purchased from Sigma-Aldrich. $(NH_4)_2TiF_6$, H_3BO_3 and PEG 400 were used as starting materials for the preparation of NH_4TiOF_3.[10] Manganese acetate tetrahydrate, $Mn(OAc)_2{\cdot}4H_2O$, was chosen as the doping agent. All these reagents were used without further purification. The NH_4TiOF_3 precursor was synthesized according to the following procedure. $(NH_4)_2TiF_6$ (0.594 g) and H_3BO_3 (0.372 g) in a molar ratio of 1 : 2 were dissolved sequentially in distilled water (30 ml) with constant stirring. Next, polyethylene glycol (9.5 g) with an average mass number of 400 (PEG 400) was added in small portions to obtain a component ratio of

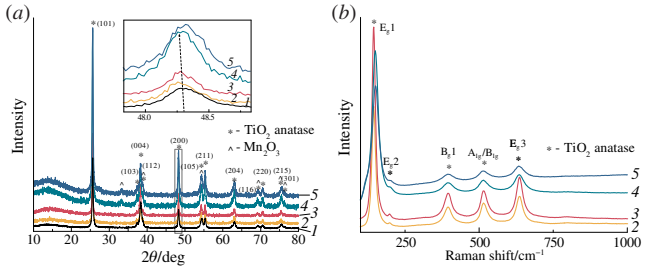

Figure 1 (*a*) XRD patterns and (*b*) Raman spectra of $Ti_{1-x}Mn_xO_2$ samples in which Mn replaces (*1*) 0, (*2*) 0.5, (*3*) 1.0, (*4*) 1.5 and (*5*) 2.0% of Ti atoms and which were obtained by heating NH_4TiOF_3 mesocrystals with the Mn precursor and PEG 400 matrix in air at a temperature of 450 °C.

0.0, 0.5, 1.0, 1.5 and 2.0% of Ti atoms, and the variable x in the $Ti_{1-x}Mn_xO_2$ formula takes values 0.0, 0.005, 0.010, 0.015 and 0.020, respectively. XRD patterns of all samples show the presence of only the anatase structure of TiO_2 [Figure 1(*a*)]. Samples with 0.5 and 1.0% of Ti atoms replaced demonstrate the absence of any impurities, while samples with 1.5 and 2.0% of Ti atoms replaced contain a small amount of MnO_y phases. Interestingly, the Raman spectra obtained from single macroparticles of all doped samples confirm the presence of only pure anatase [Figure 1(*b*)]. Specifically, all peaks at 144, 197, 399, 519 and 639 cm^{-1} correspond exactly to anatase.[12] We also performed a detailed analysis of reflections from the (200) plane, determining their positions [see Figure 1(*a*)]. The consistent shift to the left in the TiO_2 peak regions upon Mn addition implicitly indicates the incorporation of the Mn cation into the TiO_2 crystal structure (the atomic radii[13] of Ti^{4+} and Mn^{3+} are 0.605 and 0.645 Å, respectively). A significant increase in the intensity of reflections from the (004) reflections plane in all XRD patterns suggests the preferential growth of microparticles along the [001] crystallographic direction.[14]

According to SEM images, the microparticles have the shape of a regular rectangular prism with a length/width of about 3.0–6.0 μm and a height of about 0.8–2.1 μm [Figure 2(*a*)–(*d*)]. A similar shape and microstructure are demonstrated by arrays of undoped TiO_2 mesocrystals obtained with the assistance of a polymer.[12,15] Regarding the SEM image and the cross-sectional SEM image of a single microparticle of undoped anatase, the distance between layers was fixed at 15–20 nm. Individual nanoplates with a size of 30–40 nm have the shape of a rectangle and remain in the plane of basic intensity (001),[11] stacking into a rectangular macroprism [Figure 2(*e*)–(*g*)].

To understand the reason for the formation of the composite material, a number of additional analytical techniques were employed. EDX and XPS analyses [Figure 3(*b*)] consistently confirmed the presence of manganese in doped powders. XPS

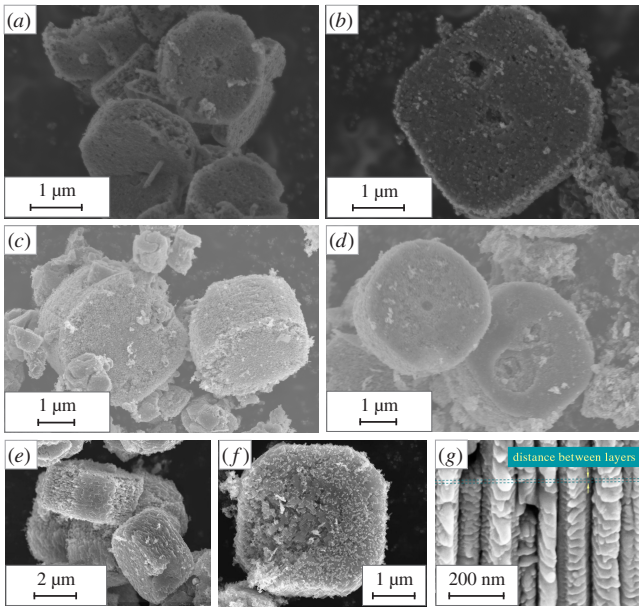

Figure 2 (*a*)–(*d*) SEM images of $Ti_{1-x}Mn_xO_2$ microparticles, in which Mn replaces (*a*) 0.5, (*b*) 1.0, (*c*) 1.5 and (*d*) 2.0% of Ti atoms and which were obtained by heating NH_4TiOF_3 mesocrystals with the Mn precursor and PEG 400 matrix in air at a temperature of 450 °C for 2 h. (*e*),(*f*) SEM images and (*g*) cross-sectional SEM image of a single microparticle of undoped TiO_2 obtained from NH_4TiOF_3 by annealing in air at 450 °C for 2 h.

became more sensitive than EDX to small amounts of Mn. In the Mn 2*p* spectrum, we identified a peak at 642 eV related to Mn^{3+} and a smaller peak at 654.4 eV related to Mn^{3+} as well. All doped powders contain double Mn 2*p* peaks separated by an energy of 12.3 eV, related to the oxidation state of Mn^{3+} [Figure 3(*a*)]. The confirmed presence of the Mn cation on the anatase surface allowed us to expect a change in PCA compared to undoped anatase mesocrystals.

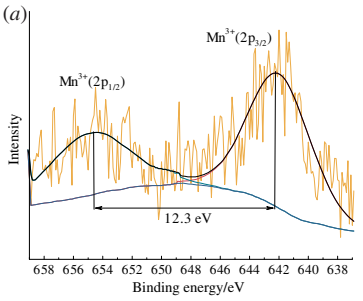

(*b*)

Batch Mn (at%)	EDX Mn (%)	XPS Mn (%)
0.5	–	0.8
1	–	1.6
1.5	1.7	2.0
2	2.5	4.3

Figure 3 (*a*) XPS spectrum of TiO_2 powder doped with 1.5% Mn. (*b*) EDX and XPS data for Mn-doped samples.

1 : 2 : 8. After complete dissolution of the polymer, the viscous solution was kept at a constant temperature of 35 °C for 20 h. The resulting product was washed from impurities by centrifugation (5 min at 6000 rpm) three times with water, and then three times with acetone. After drying at air, a sample of NH_4TiOF_3 was obtained. At the second stage, the resulting powder with or without the calculated amount of $Mn(OAc)_2{\cdot}4H_2O$ was annealed in an air atmosphere at 450 °C for 2 h and then cooled.

Scanning electron microscopy (SEM) and X-ray microanalysis (EDX) of the samples were carried out on a Carl Zeiss NVision 40 scanning electron microscope equipped with an Oxford Instruments X-Max analyzer (80 mm^2). To determine the size distribution of mesocrystals and nanoparticles, selected images of random areas of samples or mesocrystals were measured manually using the free ImageJ software.

Powder X-ray diffraction (XRD) data were recorded using a Tongda TD-3700 diffractometer (40 kV, 30 mA, CuKα radiation, linear PSD detector) operating in Bragg–Brentano geometry. Identification of diffraction maxima was carried out using the ICDD data bank. The crystal lattice parameters were refined using the free Jana2006 software package.

Raman spectroscopy of the samples was carried out using a Renishaw InVia Raman spectrometer-microscope at an exciting laser wavelength of 633 nm.

X-ray photoelectron spectroscopy (XPS) was performed on a SPECS Surface Nano Analysis spectrometer with Mg Kα excitation (1253.6 eV).

The method of low-temperature nitrogen sorption was implemented on a QuantaChrome NOVA 4200B device. Data processing was carried out using the 5-point Brunauer–Emmett–Teller (BET) model.

The PCA of the mesocrystals was measured using the triphenylmethane dye, crystal violet, as the decomposing substance. A dye solution (10^{-4} M) was added to the suspension of the powder under study, and then the resulting system was stirred in the dark until sorption equilibrium was achieved. Next, the solution in the cell was irradiated with an Ocean Optics HPX-2000 deuterium-halogen lamp (power 1.52 mW) at a temperature of 37 °C. An Ocean Optics QE65000 spectrophotometer was used to measure the concentration.

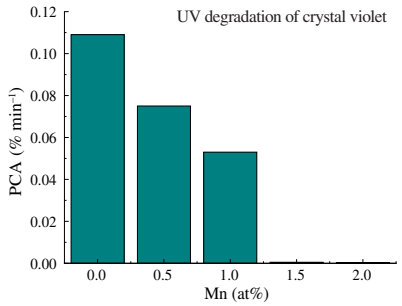

Figure 4 Photoactivity under UV irradiation of the resulting undoped and Mn-doped powders.

The results of a study of UV photodegradation of crystal violet in the presence of $Ti_{1-x}Mn_xO_2$ samples (Figure 4) indicate that increasing the dopant content predictably suppresses PCA,[16] which fades after exceeding 1.5 at% Mn. This loss of activity occurred while maintaining mesocrystalline structural integrity and with the same surface area as assessed by BET. The estimated average surface area of undoped and doped powders is about 10–15 m^2 g^{-1}.

In summary, we propose simple procedures for the synthesis of anatase TiO_2 with layered structure assisted by PEG 400 matrix powder and the fabrication of anatase-based photocatalyst doped with up to 2.0% Mn. For the first time, the distance between layers of a TiO_2 array was visualized and determined. Mn-doped TiO_2 powders may be of interest for the fabrication of low-cost photocatalyst. The highest degree of crystal violet degradation is observed for the powder with a dopant concentration of 0.5 at%. Finally, up to 1.0%, the layered Mn-TiO_2 composite is single-phase, which can be useful for studying phase mixtures of manganese and titanium oxide powders.

O.V.B., I.N.Z. and A.Y.T. acknowledge the financial support from the Russian Science Foundation (grant no. 22-29-00963). SEM analysis was performed on the equipment of the JRC PMR IGIC RAS. The authors are thankful to the Shared Use Center ‘Center of Physical and Physicochemical Methods of Analysis and Study of the Properties and Surface Characteristics of Nanostructures, Materials, and Products’ of the UdmFRC UB RAS and the Development Program of M. V. Lomonosov Moscow State University for partial support of instrumental research.

References

1 W. Choi, *Catal. Surv. Asia*, 2006, **10**, 16.
2 Y.-H. Wu, Y.-N. Lu, L.-J. Ma, H. Chen, Y.-X. Wang, W.-Q. Wu, B.-X. Lei and Z.-F. Sun, *J. Phys. Chem. C*, 2021, **125**, 1684.
3 S. Li, Z. Ma, L. Wang and J. Liu, *Sci. China, Ser. B: Chem.*, 2008, **51**, 179.
4 X. Liu, J. Zheng, K. Peng, G. Qin, Y. Yang and Z. Huang, *J. Environ. Chem. Eng.*, 2022, **10**, 107390.
5 X. Kuang, X. Deng, Y. Ma, J. Zeng, B. Zi, Y. Zhang, J. Zhang, B. Xiao and Q. Liu, *J. Mater. Chem. C*, 2022, **10**, 6341.
6 B. Bharati, N. C. Mishra, A. S. K. Sinha and C. Rath, *Mater. Res. Bull.*, 2020, **123**, 110710.
7 S. Deki, Y. Aoi, Y. Asaoka, A. Kajinami and M. Mizuhata, *J. Mater. Chem.*, 1997, **7**, 733.
8 S.-L. Chiam, S.-Y. Pung and F.-Y. Yeoh, *Environ. Sci. Pollut. Res.*, 2020, **27**, 5759.
9 L. Wang, X. Zhang, P. Zhang, Z. Cao and J. Hu, *J. Saudi Chem. Soc.*, 2015, **19**, 595.
10 O. Boytsova, I. Dovgaliuk, D. Chernyshov, A. Eliseev, P. O’Brien, A. J. Sutherland and A. Bosak, *J. Appl. Crystallogr.*, 2019, **52**, 23.
11 O. Boytsova, I. Zhukova, A. Tatarenko, T. Shatalova, A. Beiltiukov, A. Eliseev and A. Sadovnikov, *Nanomaterials*, 2022, **12**, 4418.
12 O. V. Boytsova, A. A. Sadovnikov, K. E. Yorov, A. N. Beltiukov, A. E. Baranchikov, V. K. Ivanov, X. Zhong, D. J. Lewis, P. O’Brien and A. J. Sutherland, *CrystEngComm*, 2017, **19**, 3281.
13 R. D. Shannon, *Acta Crystallogr., Sect. A: Cryst. Phys., Diffr., Theor. Gen. Crystallogr.*, 1976, **A32**, 751.
14 Q. Shi, Y. Li, E. Zhan, N. Ta and W. Shen, *CrystEngComm*, 2014, **16**, 3431.
15 O. V. Boytsova, A. E. Baranchikov, A. D. Yapryntsev, A. V. Garshev and V. K. Ivanov, *Russ. J. Inorg. Chem.*, 2018, **63**, 567 (*Zh. Neorg. Khim.*, 2018, **63**, 533).
16 I. V. Kolesnik, V. A. Lebedev and A. V. Garshev, *Nanosyst.: Phys., Chem., Math.*, 2018, **9**, 401.

Received: 5th December 2023; Com. 23/7330